

RSC Advances



This is an *Accepted Manuscript*, which has been through the Royal Society of Chemistry peer review process and has been accepted for publication.

Accepted Manuscripts are published online shortly after acceptance, before technical editing, formatting and proof reading. Using this free service, authors can make their results available to the community, in citable form, before we publish the edited article. This *Accepted Manuscript* will be replaced by the edited, formatted and paginated article as soon as this is available.

You can find more information about *Accepted Manuscripts* in the [Information for Authors](#).

Please note that technical editing may introduce minor changes to the text and/or graphics, which may alter content. The journal's standard [Terms & Conditions](#) and the [Ethical guidelines](#) still apply. In no event shall the Royal Society of Chemistry be held responsible for any errors or omissions in this *Accepted Manuscript* or any consequences arising from the use of any information it contains.

Ab initio calculations of quantum transport of Au-GaN-Au nanoscale junctions

T. Zhang ¹, Y. Cheng ^{1,*}, and X. R. Chen ^{1,2,*}

¹ Institute of Atomic and Molecular Physics, College of Physical Science and Technology,

Sichuan University, Chengdu 610065, China;

² International Centre for Materials Physics, Chinese Academy of Sciences, Shenyang 110016, China

Abstract: We investigate the contact geometry and electronic transport properties of a GaN pair sandwiched between Au electrodes by performing density functional theory plus the non-equilibrium Green's function method. The Au-GaN-Au junctions breaking process is simulated. We calculate the corresponding cohesion energy and obtain the equilibrium conductance and the projected density of states of junctions. We also calculate the pulling force of the four configurations, and the spatial electron density difference after the junctions is broken. In addition, the current of junctions is computed under small bias. It is found that that all junctions have large conductance showing a non-linear I - V relationship.

Key words: Electronic transport; Density functional theory; Non-equilibrium Green's function; GaN

* Corresponding authors. y.cheng@scu.edu.cn (Y. Cheng); xrchen@scu.edu.cn (X. R. Chen)

1. Introduction

The molecular electronics [1,2] has become a hot topic in physics and materials science in the last decade. To develop the molecular electronics, it is essential to understand quantitatively the electronic transports of molecular junctions between two metallic electrodes. When the molecule is attached to metallic electrodes, the electronic current will turn more complex. However, with the development of micro-fabrications and self-assembly techniques, it has become a reality for designing a molecule device or controlling the electronic transport properties on a nanoscale system [3].

The electronic transports through single-atomic contacts [4] and molecules [5] are of great fundamental interest since they might be applicable in future electronic and energy-conversion devices based on electron transfer, shot noise, heat transport, negative differential resistance, gate controlled, and so on. By trapping a single molecule in break junctions (MCBJ) formed by mechanical strain [6], electromigration [7] and scanning tunneling microscopes (STM) [8], the current-voltage (I - V) characteristic of single molecules has been extensively investigated. Remarkable progress in the experimental growth, control, and characterization techniques at the nanoscale has allowed producing many potentially useful molecular electronic devices, such as molecular wires, resonant tunneling diodes, molecular switches, molecular rectifiers, and molecular storage devices [9-22]. Certainly, the theories also play a fundamental role in explaining these experiments and designing new ones [23,24].

Recently, there is a strong motivation for examining the transport properties of Group III nitride based nanowires for possible applications in low-power and high-density

field-effect transistors (FETs), solar cells, terahertz emitters, and detectors [25, 26]. Their outstanding physical and chemical stability enables the III-N devices to be operated under extreme environmental conditions. Huang *et al.* [25] reported successfully the fabrication of logic gates and demonstrated the computation capabilities from assembled nanowire p-Si and n-GaN crossed nanowire junctions. Later, Renard *et al.* [26] showed that the polar GaN/AlN axial heterostructures in nanowires grown by plasma-assisted molecular-beam epitaxy were subject to a clear quantum-confined Stark effect. They addressed the transport properties of the n-type GaN/AlN double-barrier nanowires.

In this work, we will focus on the effects of molecular contact geometry on the conductance and the I - V characteristics of the GaN molecule sandwiched between Au electrodes. We simulate the Au-GaN-Au junctions breaking process in the four different anchoring geometries, and calculate the I - V characteristics of the junctions at the equilibrium positions. The rest of the paper is organized as follows. The theoretical methods and the computational details are given in Section 2. Some results and discussion are presented in Section 3. Finally, the summary of our main results are given in Section 4.

2. Theoretical method and calculation details

Our theoretical investigations for the electronic structure properties are based on the *ab initio* density functional theory (DFT) as implemented in the Siesta code [27]. This method employs a linear combination of pseudo-atomic orbitals for the basis set and replaces the atomic cores by nonlocal norm-conserving Troullier-Martins pseudo-potentials [28], factorized in the Kleinman-Bylander form [29]. In our calculations,

we use the Perdew-Zunger form [30] of the local-density approximation (LDA) to the exchange-correlation functional. Nonlocal scalar-relativistic Troullier-Martins pseudo-potentials are generated from the configurations: Au ($5d^{10}6s^1$), Ga ($4s^24p^1$), and N ($2s^22p^3$). A single-zeta is used as the basis set for Au, and a double-zeta basis is adopted for the orbitals of the other species (Ga and N).

The transport calculations have been performed with the *ab initio* transport code Smeagol [31-33], which is used to calculate the density matrix and the transmission coefficients of a two probe device using the non-equilibrium Green function (NEGF) formalism. The physical model is divided into three parts, namely left and right semi-infinite Au (1 0 0) metal electrodes and the central region. The latter contains the GaN molecule plus parts of the Au electrodes accommodating the molecule-surface interaction (see Fig. 1). The two semi-infinite leads are assumed to be in equilibrium with well-defined chemical potentials and act as current/voltage probes. Notice that the left and the right electrodes are considered perfect crystal and the chemical potential is well approximated by that of a perfect bulk electrode. In contrast, the electronic potential of the scattering region is calculated self-consistently for each applied bias [34-36]. For this purpose we define the Green's function of the scattering region in the presence of the leads as:

$$\hat{G} = \lim_{\delta \rightarrow 0} [(E - i\delta)\hat{S} - \hat{H}_S[\rho] - \hat{\Sigma}_L - \hat{\Sigma}_R]^{-1}, \quad (1)$$

where $\hat{H}_S[\rho]$ is DFT Hamiltonian, \hat{S} is the corresponding overlap matrix, E is the energy and $\hat{\Sigma}_L$ and $\hat{\Sigma}_R$ are the self-energies, respectively, for the left and right lead. This allows us to evaluate the density matrix

$$\rho = \int \frac{dE}{2\pi} \hat{G}[\hat{\Gamma}_L f(E - \mu_L) + \hat{\Gamma}_R f(E - \mu_R)] \hat{G}^+, \quad (2)$$

With $\hat{\Gamma}_\alpha = i[\hat{\Sigma}_\alpha - \hat{\Sigma}_\alpha^\dagger]$. Since the DFT Hamiltonian H_S depends solely on the density matrix, Eqs. (1) and (2) can be iterated until reaching self-consistency.

In what follows, the leads have an fcc crystalline structure and are oriented along the (1 0 0) direction. The unit cell of the extended molecule comprises a GaN molecule and 13 Au atomic layers each containing 3×3 atoms in the surface plane. A periodic boundary condition is applied in the basal plane (orthogonal to the transport direction) with four irreducible k-points in the two-dimensional Brillouin zone. The Brillouin zone is set to be $2 \times 2 \times 100$ points following the Monkhorst-Pack k-point scheme [37]. The cut-off energy and iterated convergence criterion for total energy are set to 200 Rydberg and 10^{-4} , respectively. Furthermore, the charge density is integrated over 50 energy points along the semi-circle and 20 energy points along the line in the complex plane, and 20 poles are used for the Fermi distribution.

3. Results and discussion

To gain insight into the possible structures of Au-GaN-Au junctions, we have made successive relaxations for each system by keeping all Au atoms in the leads fixed and only relaxing the apexes of the point contact in the center until the force on each atom is smaller than 0.1 eV/\AA in each optimization process [38]. The ground state energy is calculated as a function of the distance d_z between the outer surface layers (not relaxation) (Fig. 1), thereby simulating the contact formation in a mechanically controlled break junction (MCBJ) experiment. We increase/decrease all atomic distances between them

proportionally to change the distance d_z between the two Au (1 0 0) surface, and subsequently the system is relaxed to form the equilibrium structure. In the following, we concentrate on four different structures for the gold contacts as shown in Fig. 1: (a) GaN connected to pyramidal-shaped electrodes at the top site with the molecular axis parallel to the transport direction(z -axis), (b) GaN connected to the pyramidal-shaped electrodes at the hollow site to the left and at the top site to the right (molecular axis parallel to z-axis), (c) GaN connected to the pyramidal-shaped electrodes at the top site to the left and at the hollow site to the right (molecular axis parallel to z-axis), and (d) GaN connected to two hollow sites with the molecular axis parallel to z.

The calculated conductance as a function of distance d_z is shown in Fig. 2. This conductance G associated to the two-probe device can be calculated by using Fisher-Lee's relation [39]

$$G = \frac{2e^2}{h} \text{Tr}[\Gamma_L G_M^{R+} \Gamma_R G_M^R] = \frac{2e^2}{h} T(E), \quad (3)$$

where the $\Gamma_{L/R}$ is the anti-hermitian part of the self energy, G_M^R , which contains all the information about the electronic structure of the extended molecule attached to the leads, is the retarded Green's function of the scattering region, e is electron charge and h is the Planck's constant. $T(E)$ is the simple energy-dependent total transmission coefficient of standard scattering theory [40]. For firstly the GaN top-top structure, as the junctions are stretched, the conductance shows a little change from $1.42 G_0$ ($G_0 = 2e^2/h$ is the conductance quantum) at $d_z \sim 13.072 \text{ \AA}$ to $1.34 G_0$ at $d_z \sim 13.872 \text{ \AA}$, and then slightly increases to $1.63 G_0$ at 15.072 \AA , but at 15.872 \AA , the conductance declines rapidly to 0, which is the break point of Ga-N bond. For configuration (b), the conductance decreases

from $2.21 G_0$ at $d_z \sim 8.631 \text{ \AA}$ to $1.52 G_0$ at $d_z \sim 11.831 \text{ \AA}$ as the two contact distance is pulled apart, and then jumps abruptly to 0 at $d_z \sim 12.231 \text{ \AA}$, which is the break point of N-Ga bond. For configuration (c), with junction stretched, the conductance decreases from $0.78 G_0$ at $d_z \sim 9.432 \text{ \AA}$ to $0.60 G_0$ at $d_z \sim 8.632 \text{ \AA}$, and then abruptly declines to $0.067 G_0$ at $d_z \sim 8.232 \text{ \AA}$, which is the break point of Au-Ga bond. Finally, for the configuration (d), with the increase of distance, the conductance firstly begins to increase from $3.30 G_0$ at $d_z \sim 10.191 \text{ \AA}$ to $3.38 G_0$ at $d_z \sim 10.591 \text{ \AA}$, and then it declines rapidly to $1.54 G_0$ at $d_z \sim 10.991 \text{ \AA}$, and jumps abruptly from $1.34 G_0$ at $d_z \sim 12.991 \text{ \AA}$ to $0.27 G_0$ at $d_z \sim 13.391 \text{ \AA}$, which is the break point of Ga-N bond. In the whole process, it is easy to see that, the conductance decreases with junctions stretched in the four configurations except some unstable stations. It indicates that the conductance of junction is sensitive to the variation of the two contact distance and anchoring geometries. Namely it shows the sensitivity of the conductance to the local atomic re-arrangement of the contact region [41]. Such behavior is characteristic of the phase-coherent transport regime and a direct manifestation of the wave nature of the charge carriers.

As the two contact distance is pulled apart, the interaction force between atoms also shows the corresponding change. In Fig. 3, we present the pulling force as a function of the electrodes' separation, which is calculated as $F_z = dE_{total} / d\Delta L$, where E_{total} (Au electrodes + GaN molecule) is the total energy of the system at each stretch and ΔL stands for the elongation of the system. In fact, the pulling force as a function of d_z is characterized by elastic stages (where the force increases) followed by stress release. The existence of negative force means that the system is under compressive strain. For the

configuration (a) the Ga-N bond is compressed at a small d_z (< 13.5 Å), and the Ga-N bond-length gets stretched as the distance d_z is beyond 13.5 Å. Its maximum achieved force is calculated to be 3.70 nN, implying that Ga-N bond can't be stretched further when d_z is larger than 15.872 Å. This is consistent with the obtained result by analyzing the calculated conductance as a function of d_z . For the configurations (b), (c), and (d), the maximum achieved force is 2.98 nN at 11.031 Å (Au-N), 2.46 nN at 11.832 Å (Ga-Au), and 3.61 nN at 8.991 Å (Ga-N), respectively. The calculated results show that the strength of Ga-N bond is stronger than other bonds including the Ga-Au, and N-Au bonds. Although we find that out of four studied structures two structures break exactly at the Ga-N bond, the phenomenon can be put down to the reason that the Au atom and the N atom (Ga atom) have the different coordination numbers in the structure (a) and (d). In the structure (b), the Ga atom and Au atom have the same coordination number of 5, that is to say, the Ga atom and the Au atom lie on the same statue. The broken bond is the weak bond (N-Au) as the two contact distance is pulled apart continuously, which is similar to the structure (c) whose broken bond is the weak (Ga-Au) bond. However, in the structure (a) whose Au atom has the higher coordination number when compared to the Ga (N) atom, the broken bond is the Ga-N bond rather than the weak bond. The coordination atoms around the Au atom have the weak interaction with the N (Ga) atom, and in consideration of the tiny difference of the strength between the Au-N (Ga) bond and N-Ga bond, the superposition of the weak interaction and the strength of Au-N (Ga) bond can exceed the strength of the N-Ga bond. Hence, for the structure (a) and (d), the broken bond is the N-Ga bond.

Additionally, we also calculate the spatial electron density difference when the pulling force is beyond the corresponding maximum achieved force (structural break) for the four configurations, which is illustrated in Fig. 4. The electron density difference, $\rho'(\mathbf{r}) = \rho(\mathbf{r}) - \rho_{atoms}(\mathbf{r})$, between the self-consistently calculated electron density of the junctions after structural break, $\rho(\mathbf{r})$, and that of free atoms placed at the same positions, $\rho_{atoms}(\mathbf{r})$, describes how uneven the distribution of valence electrons of the junctions is after structural break. For the configuration (a), the electrons are distributed uniformly between the Au atom and Ga atom, Ga atom and N atom, and N atom and Au atom, meaning that they form the strong covalent bonding with the nearest-neighboring atoms. Such behavior is similar to that of the configuration (d). By observing the charge densities of the configurations (b) and (c), it can be found that the charge is more localized on the Ga/N atom rather than the right/left Au atom, which may be put down to the reason that Ga and N atoms have a stronger electronegativity.

To calculate the most stable structures for the four different configurations in different distances, we calculate the cohesion energy as a function of d_z during the simulation process. The cohesion energy is defined as follows: $E = E(\text{Au electrodes} + \text{GaN molecule}) - E(\text{GaN molecule}) - E(\text{Au electrodes})$. The results of the calculation are shown in Fig. 2. It is found that there is a similar parabola in the curve of the total energy as a function of the distance d_z for the four configurations. The minimum energy in every curve is located at the equilibrium distances. If the electrodes are free to relax, the system will naturally form the equilibrium structure with the equilibrium distance $d_{z,eq}$ corresponding to those energy minima. It can be found that, for the four different

structures (a), (b), (c) and (d), its equilibrium distance is $d_{z,eq} = 14.272 \text{ \AA}$, 11.031 \AA , 9.832 \AA and 7.791 \AA , respectively. When the junctions are located at the optimal equilibrium positions, the Ga-N bond-length, d_{Ga-N} , is 1.873 \AA for configuration (a), 1.900 \AA for configuration (b), 1.951 \AA for configuration (c) and 2.011 \AA for configuration (d). The calculated results of Ga-N bond-length are also consistent with the calculated result (1.87 \AA) of Song *et al.* [42]. In short, it is not difficult to find that the cohesion energy of the two probe systems at the optimal position is different in these four configurations. From the calculated results, it is also easy to see that the cohesion energy of the system increases in turn from configuration (a) to (d), and the equilibrium conductance of GaN in these four configurations at the optimal position is $1.50 G_0$ for configuration (a), $1.75 G_0$ for configuration (b), $0.61 G_0$ for configuration (c), and $1.54 G_0$ for configuration (d). In fact, the conductance values are the direct consequence of the small energy difference between the electrodes' Fermi energy E_F and the molecular orbital which dominates HOMO or LUMO. The Kohn-Sham orbitals are mathematical objects rather than true molecular orbitals, hence their energy should be shifted [43] which leads to the result that the calculated value of conductance may be larger than the experimental value. There are some studies on single-molecule junctions in a solvent that consider the energy offset of the dominant molecular orbital relative to the electrode Fermi level, which get very meaningful results [44,45]. Unfortunately, there is no experimental value of conductance of the GaN molecule to compare with. But we expect that our theoretical prediction might be useful in further experiments and theories.

To further understand the conductance of Au-GaN-Au junctions, we can analyze the

transmission spectrum $T(E, V=0)$ (Fig. 5) and the projected density of states (PDOS) (Fig. 6) of the GaN molecule. For the configuration (a), E_F of Au is located at a peak in the transmission function. Thus, $T(E_F, 0)$ is dominated by a resonance corresponding to the energy of the highest occupied molecular orbital (HOMO), ϵ_{HOMO} . This provides a large conductance, so the Au-GaN-Au junctions have a large transmission. Such a transport channel is almost formed by p_x and p_y orbital electrons of Ga and N atoms, with an almost negligible contribution from their p_z . For the configuration (b), the Ga atom on the side binds at the hollow site of the Au (1 0 0) surface, and for (c), the N atom on the side binds at the hollow site. Both their electronic coupling are considerably stronger than that in configuration (a), which leads to a strong broadening and shift of the resonances. The transmission becomes flat around the Fermi level. But it is not difficult to find that the configuration (c) have a stronger electronic coupling than (b) by observing the broadening degree of HOMO in the transmission spectrum. The Fermi level is located just above the HOMO for (b), with a stronger resonant effect in the transmission spectrum. Hence the HOMO contributes much to G so that (b) has the largest transmission among all the junctions. Its transport channel is mainly formed by the p_x and p_y orbits of the Ga and N atoms, a little p_z of the N atom, and s orbital electrons of the Ga atom. For (c), the stronger electronic coupling induces the HOMO of GaN to broaden to a point where it becomes indistinguishable in the PDOS. As a consequence, there is no resonance at E_F , but instead, $T(E)$ is flat and featureless. This phenomenon is more obvious for configuration (d) due to the reason that (d) has the strongest electronic coupling.

The current is self-consistently calculated within the non-equilibrium Green's

function approach with the voltage-dependent Landauer formula [36]

$$I = \frac{2e}{h} \int \text{Tr}[\Gamma_L G_M^{R+} \Gamma_R G_M^R] [f(E - \mu_L) - f(E - \mu_R)] dE \quad (4)$$

$$f(E - \mu_{L,R}) = 1 / \{ \exp[(E - \mu_{L,R}) / k_B T] + 1 \}, \quad (5)$$

where k_B is the Boltzmann constant, T is the temperature and f is the Fermi-Dirac distribution function of two electrodes with the chemical potential $\mu_{L/R}$ for the left/right electrode. The result of relationship between current and bias voltage are shown in Fig. 7. In agreement with the experiment, the I - V of the asymmetric molecule is asymmetric with respect to voltage inversion. This asymmetry can be due to an asymmetry in either the leads or in its couplings to the molecule. The latter factor can be due to an intrinsic property of the molecule. Hence, the asymmetric shape of I - V curves is rationalized for the four configurations. Additionally, for the configuration (b), in the low bias zone from -0.15 V to 0.2 V, GaN molecule displays a colossal resistance (dV/dI) effect, but in higher bias region ($|V| > 0.2$ eV), the situation is reversed, i.e. the conductance (dI/dV) of the configuration (b) abruptly increases and is larger than that of other configurations. Such behavior is similar to that of the configuration (a), which can be seen from Fig. 7(i). Conversely, for the configurations (c) and (d) shown in Fig. 7(ii), the conductance is higher at the lower bias zone than that at higher bias region. Hence for the four configurations, their I - V curves show a non-linear behavior, indicating that the junctions have a semiconductor-like characteristic.

To achieve a qualitative understanding of the underlying physics, it is useful to calculate the transmission coefficients as a function of the energy for different biases and configurations, because the current through the system is proportional to the integral of the

transmission coefficients in the energy window ($E_F - eV/2, E_F + eV/2$). The calculated transmission spectrum of $T(E)$ is shown in Fig. 5, under the bias of 0 V, 0.4 V, 0.8 V, 1.2 V. For the configuration (a), we can observe a significant drift of the HOMO resonance to lower energies as the bias increases. Such a drift of the HOMO makes the HOMO away from the Au Fermi level. Because the transmission peak does not leave the energy window, the current and conductance remains relatively large. In contrast to the configuration (b), little change happens to the transmission coefficient around the Fermi level as the bias increases. For the remaining configurations (c) and (d), we can find the similar phenomenon: with the increasing bias, the HOMO of GaN gradually broadens. As a consequence, there is no resonance at E_F , but instead, $T(E)$ becomes flat and featureless.

4. Conclusions

In summary, we have applied the density functional theory plus the non-equilibrium Green's function method to systematically investigate the transport properties of a GaN molecule sandwiched between two semi-infinite Au (1 0 0) metal electrodes in the four different anchoring configurations. We have simulated the Au-GaN-Au junctions breaking process and calculated the corresponding cohesion energy in the four different configurations. The obtained conductance of GaN in four configurations at the optimal position is $1.50 G_0$, $1.75 G_0$, $0.61 G_0$ and $1.54 G_0$, respectively. It can be found that the molecular-scale contact geometry plays a critical role in the absolute value of the conductance. By calculating the pulling force of the four configurations, and their spatial electron density differences after structural break, we can conclude that the Ga-N bond is

stronger than other bonds including Au-Ga bond and Au-N bond. Additionally, we have also calculated the current of junctions at the optimal position under small bias for the four configurations. It is found that: for the configurations (a) and (b), the conductance (dI/dV) is smaller under the lower bias zone than that under the higher bias region, and for the configurations (c) and (d), the situation is reversed. Such behavior shows that the GaN junctions have the characteristic of the semiconductor-like junction.

Acknowledgments

The authors would like to thank Dr. S. Sanvito for his providing us the SMEAGOL code. We also thank the support by the National Natural Science Foundation of China under Grant Nos. 11174214 and 11204192 and the NSAF under Grant No. U1430117 and U1230201.

References

- [1] H. Song, M. A. Reed and T. Lee, *Adv. Mater.*, 2011, **23**, 1583.
- [2] C. Joachim, J. K. Gimzewski and A. Aviram, *Nature*, 2000, **408**, 541.
- [3] D. R. Bowler, *J. Phys.: Condens. Matt.*, 2004, **16**, R721.
- [4] F. T. Liu, Y. Cheng, F. B. Yang and X. R. Chen, *Chin. Phys. Lett.*, 2013, **30**, 107303.
- [5] P. Reddy, S. Y. Jang, R. A. Segalman and A. Majumdar, *Science*, 2007, **315**, 1568.
- [6] M. A. Reed, C. Zhou, C. J. Muller, T. P. Burgin, and J. M. Tour, *Science*, 1997, **278**, 252.
- [7] H. Parket, *Nature*, 2000, **407**, 57.

- [8] B. Xu and N. J. J. Tao, *Science*, 2003, **301**, 1221.
- [9] F. T. Liu, Y. Cheng, F. B. Yang and X. R. Chen, *Physica E*, 2014, **56**, 96.
- [10] J. X. Yu, Y. Cheng, S. Sanvito and X. R. Chen, *Appl. Phys. Lett.*, 2012, **100**, 103110.
- [11] C. J. Xia, D. S. Liu, H. C. Liu and X. J. Zhai, *Physica E*, 2011, **43**, 1518.
- [12] M. Qiu and K. M. Liew, *Phys. Lett. A*, 2011, **375**, 2234.
- [13] X. J. Liu and Z. An, *Org. Electron.*, 2011, **12**, 1352.
- [14] Y. P. An, C. L. Yang, M. S. Wang, X. G. Ma and D. H. Wang, *Curr. Appl. Phys.*, 2010, **10**, 260.
- [15] G. B. Abadir, K. Walus and D. L. Pulfrey, *J. Comput. Electron.*, 2009, **8**, 1.
- [16] P. Zhao, P. J. Wang, Z. Zhang and D. S. Liu, *Physica B*, 2010, **405**, 446.
- [17] P. Zhao, P. J. Wang, Z. Zhang, M. J. Ren and D. S. Liu, *Physica B*, 2010, **405**, 2097.
- [18] P. Zhao, Z. Zhang, P. J. Wang and D. S. Liu, *Physica B*, 2009, **404**, 3462.
- [19] P. Zhao, P. J. Wang, Z. Zhang and D. S. Liu, *Phys. Lett. A*, 2010, **374**, 1167.
- [20] C. J. Xia, D. S. Liu, C. F. Fang and P. Zhao, *Physica E*, 2010, **42**, 1763.
- [21] J. Huang, Q. Li, H. Su and J. Yang, *Chem. Phys. Lett.*, 2009, **479**, 120.
- [22] E. Zahedi and A. Pangh, *Superlatt. Microstruct.*, 2011, **50**, 386.
- [23] V. M. Garcí'a-Sua' rez, A. R. Rocha, S. W. Bailey, C. J. Lambert, S. Sanvito and J. Ferrer, *Phys. Rev. B*, 2005, **72**, 045437.
- [24] K. H. Khoo, J. B. Neaton, H. J. Choi and S. G. Louie, *Phys. Rev. B*, 2008, **77**, 115326.
- [25] Y. Huang, X. Duan, Y. Cui, L. J. Lauhon, K. H. Kim and C. M. Lieber, *Science*, 2001, **294**, 1313.
- [26] J. Renard, R. Songmuang, G. Tourbot, C. Bougerol, B. Daudin and B. Gayral, *Phys.*

Rev. B, 2009, **80**, 121305.

[27] J. M. Soler, E. Artacho, J. D. Gale, A. García, J. Junquera, P. Ordejón and D.

Sánchez-Portal, *J. Phys.: Condens. Matt.*, 2002, **14**, 2745.

[28] N. Troullier and J. L. Martins, *Phys. Rev. B*, 1991, **43**, 1993.

[29] L. Kleinman and D. M. Bylander, *Phys. Rev. Lett.*, 1982, **48**, 1425.

[30] J. P. Perdew, *Phys. Rev. B*, 1986, **33**, 8822.

[31] I. Rungger and S. Sanvito, *Phys. Rev. B*, 2008, **78**, 035407.

[32] A. R. Rocha, V. M. Garcia, S. W. Bailey, C. J. Lambert, J. Ferrer and S. Sanvito,

Nature Mater., 2005, **4**, 335.

[33] A. R. Rocha, V. M. Garcia-Suarez, S. Bailey, C. Lambert, J. Ferrer and S. Sanvito,

Phys. Rev. B, 2006, **73**, 085414.

[34] C. Caroli, R. Combescot, D. Lederer, P. Nozieres and D. Saint-James, *J. Phys. C*,

1971, **4**, 2598.

[35] L. V. Keldysh, *Sov. Phys. JETP*, 1965, **20**, 1018.

[36] S. Datta, *Electronic Transport in Mesoscopic Systems*, Cambridge University Press

Cambridge, 1995.

[37] H. J. Monkhorst and J. D. Pack, *Phys. Rev. B*, 1976, **13**, 5188.

[38] R. B. Pontes, A. R. Rocha, S. Sanvito, A. Fazzio and A. J. Roque da Silva, *ACS Nano*,

2011, **5**, 795.

[39] D. S. Fisher and P. A. Lee, *Phys. Rev. B*, 1981, **23**, 6851.

[40] M. Buttiker, Y. Imry, R. Landauer and S. Pinhas, *Phys. Rev. B*, 1985, **31**, 6207.

[41] I. S. Kristensen, D. J. Mowbray, K. S. Thygesen and K. W. Jacobsen, *J. Phys.:*

Condens. Matt., 2008, **20**, 374101.

[42] B. Song, C. H. Yao and P. L. Cao, *Phys. Rev. B*, 2006, **74**, 035306.

[43] I. Baldea, *Electrochem. Commun.*, 2013, **36**, 19.

[44] S. Y. Quek, H. J. Choi, S. G. Louie and J. B. Neaton, *Nano Lett.*, 2009, **9**, 3949.

[45] I. Baldea, *Nanoscale*, 2013, **5**, 9222.

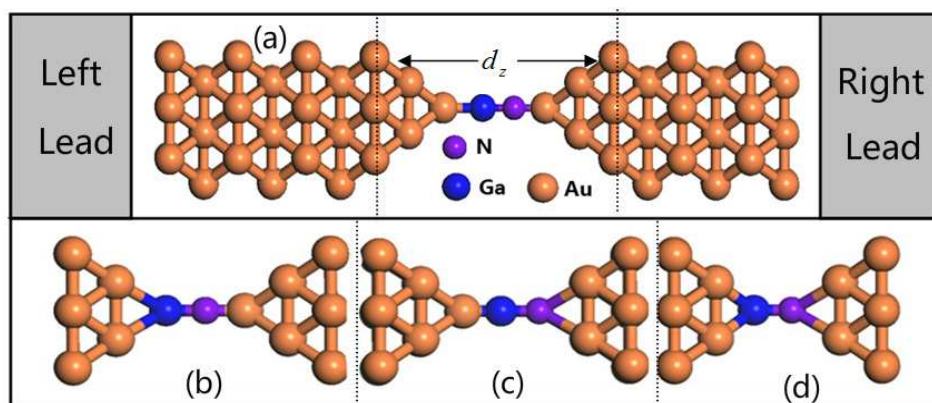
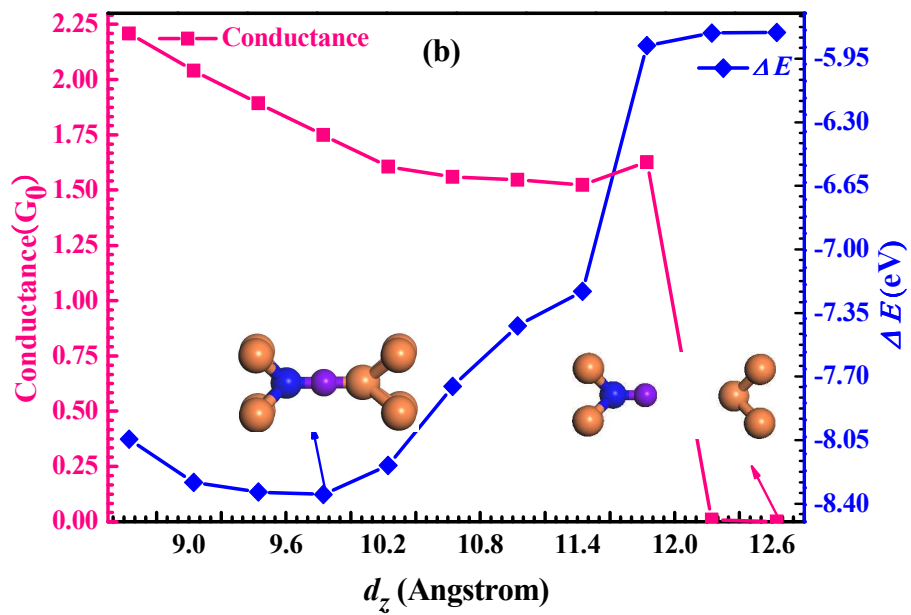
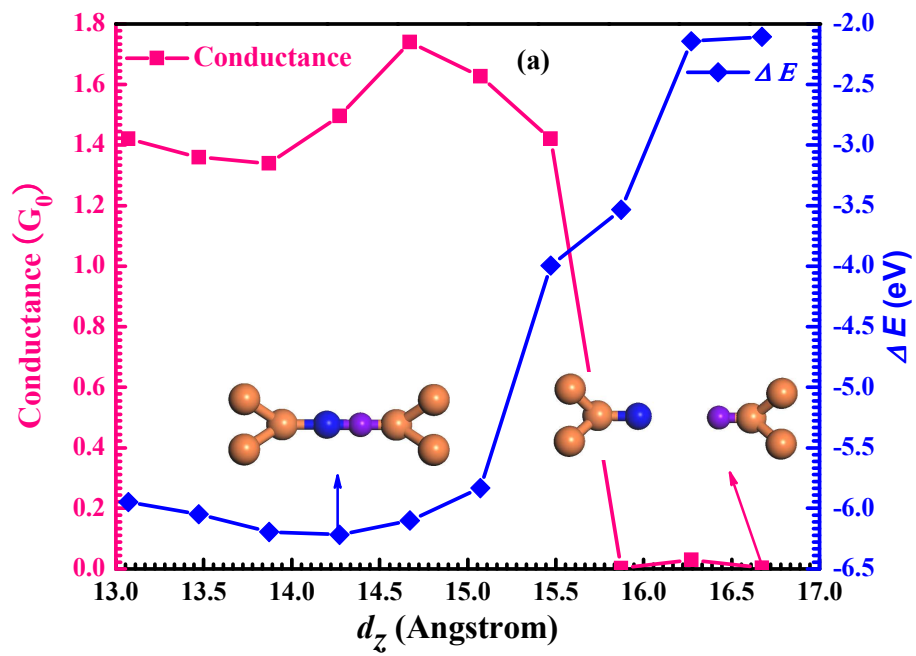


Fig. 1. The different anchoring configurations connecting Au leads and GaN molecule: (a) top–top configuration with the Ga, N bonds axis separately parallel to the transport direction (top–top parallel), (b) top–hollow configuration with the N, Ga bond axis separately, (c) top–hollow configuration with the Ga, N bond axis separately, and (d) hollow–hollow configuration.



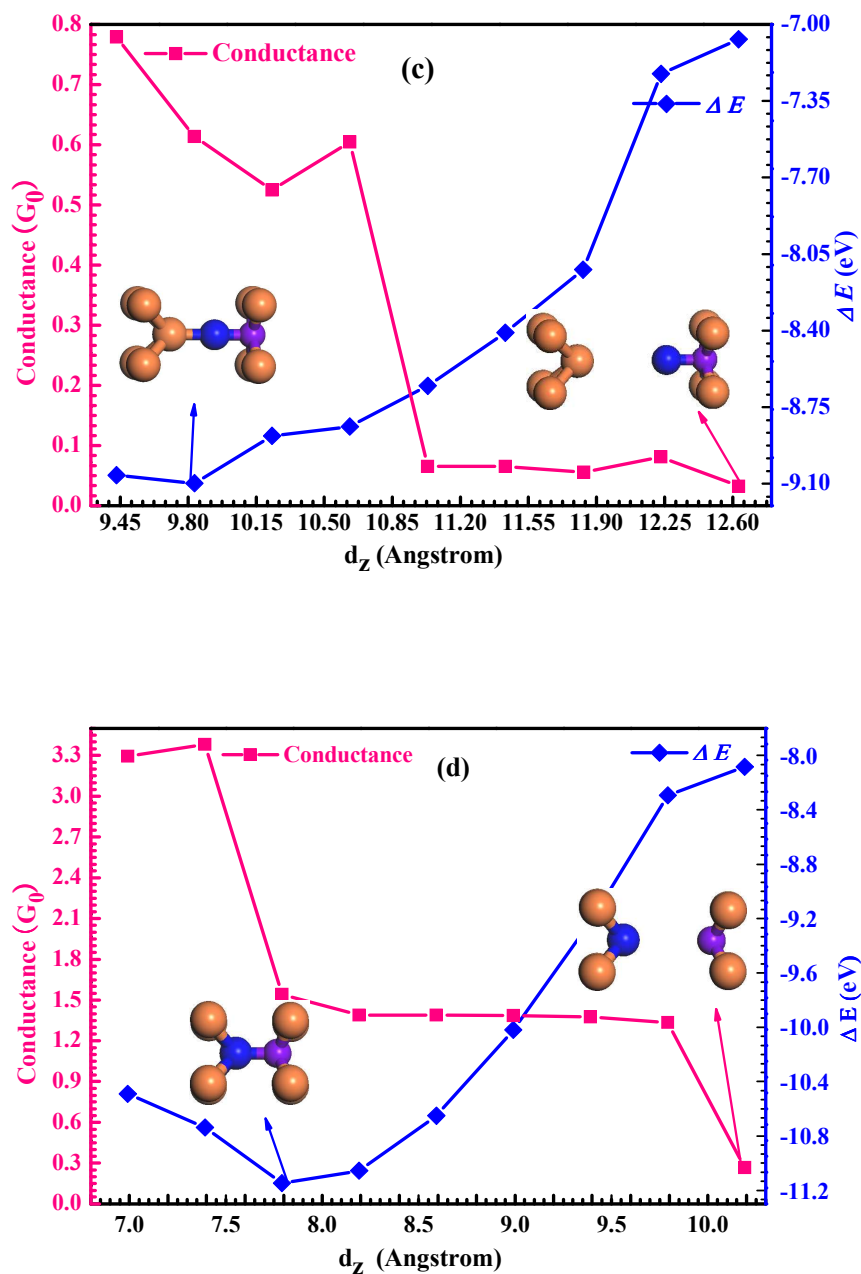


Fig. 2. Conductance (solid squares and left-hand side axis) and the cohesion energy (open squares and right-hand side axis) for the four configurations investigated as a function of distance d_z : (a) top-top parallel configuration, (b) hollow-top configuration for GaN, (c) top-hollow configuration for GaN, (d) hollow-hollow configuration

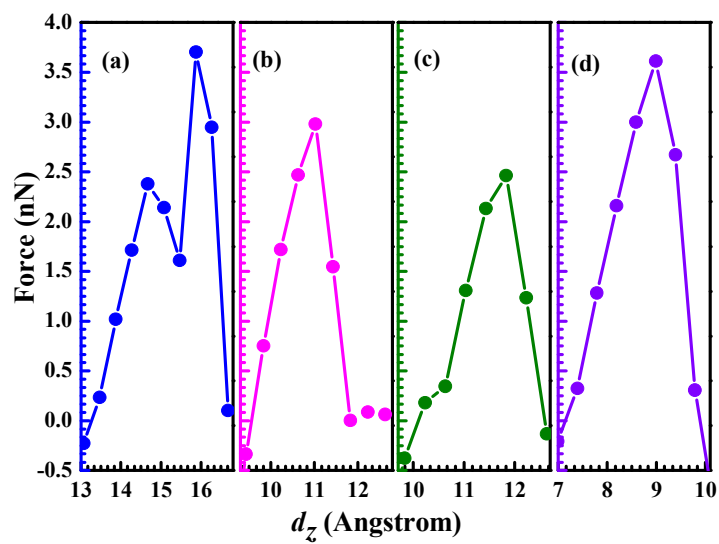


Fig. 3. The pulling force at the Fermi level calculated as a function of the electrodes' separation: (a) top-top configuration, (b) hollow-top configuration, (c) top-hollow configuration, and (d) hollow-hollow configuration.

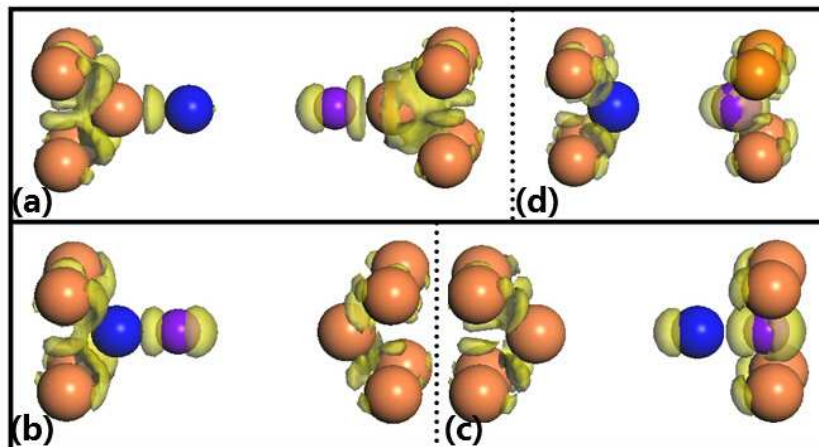
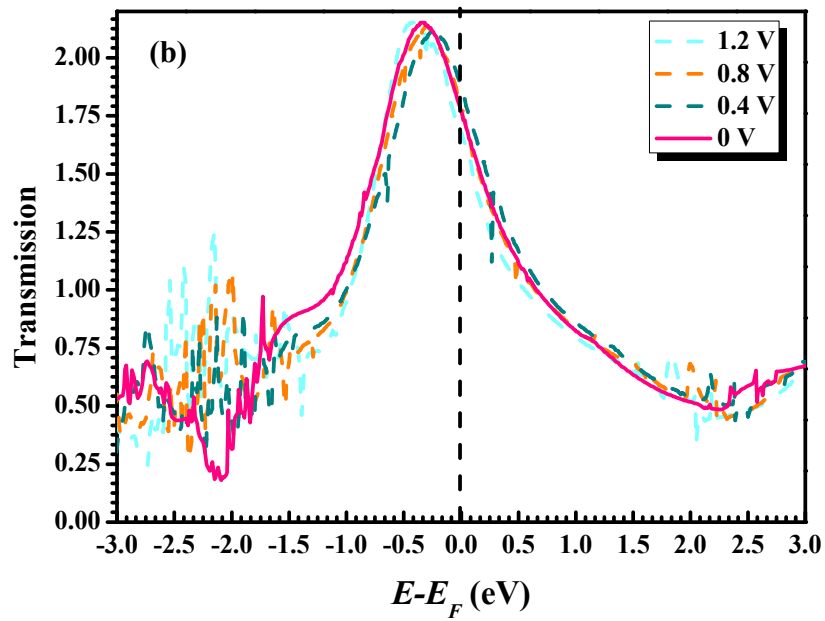
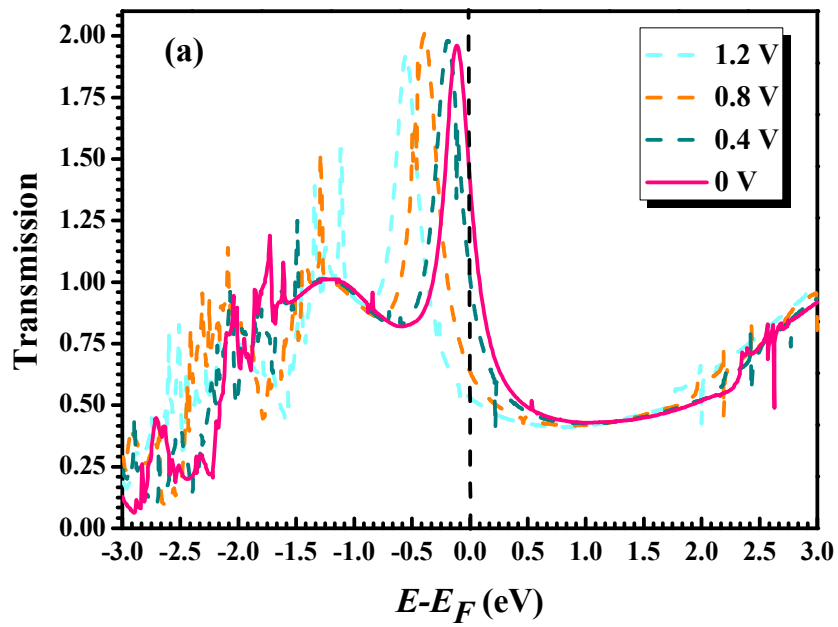


Fig. 4. Spatial electron density difference around the Fermi level of GaN molecule at the corresponding break point: (a) top-top configuration ($d_z = 16.272 \text{ \AA}$), (b) hollow-top configuration ($d_z = 12.631 \text{ \AA}$), (c) top-hollow configuration ($d_z = 12.632 \text{ \AA}$), and (d) hollow-hollow configuration ($d_z = 10.191 \text{ \AA}$).



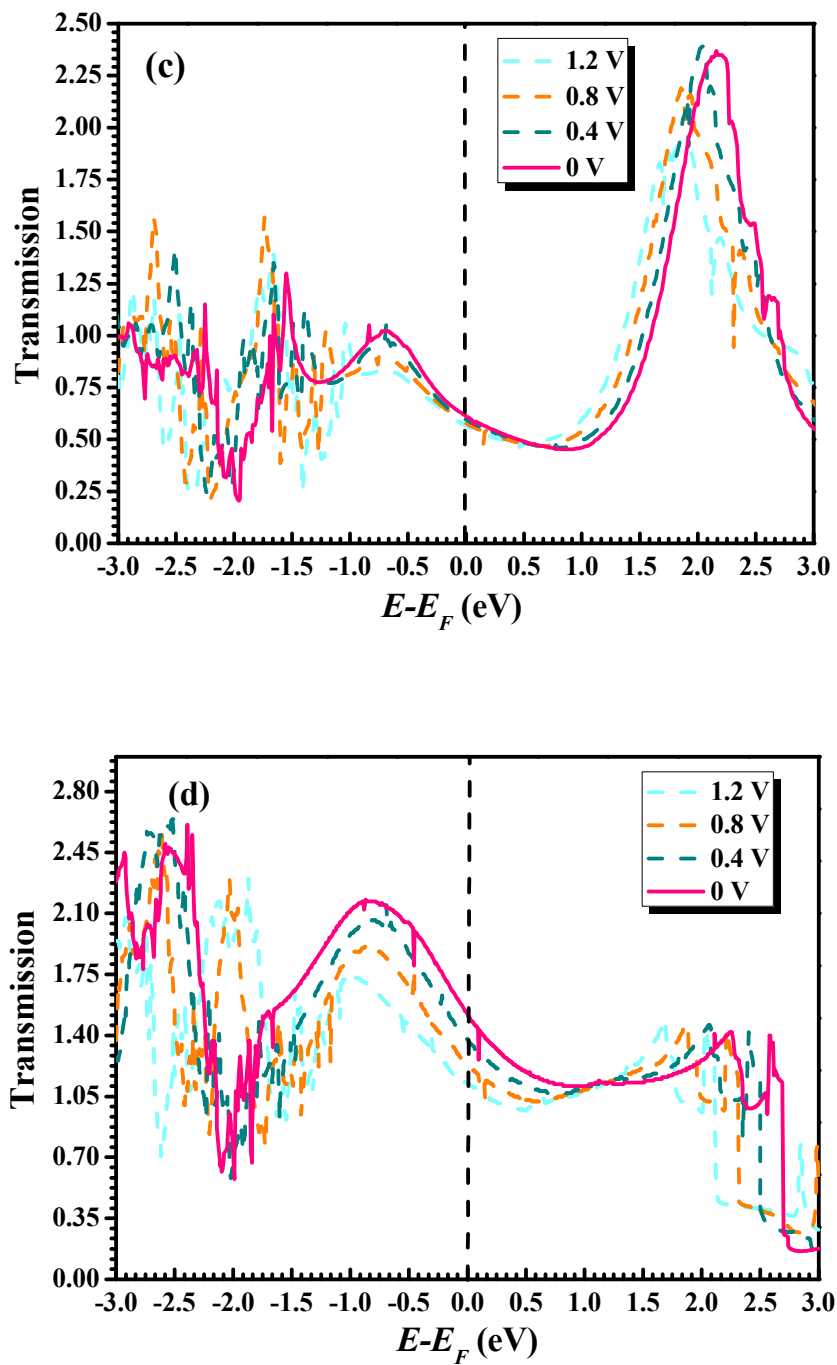
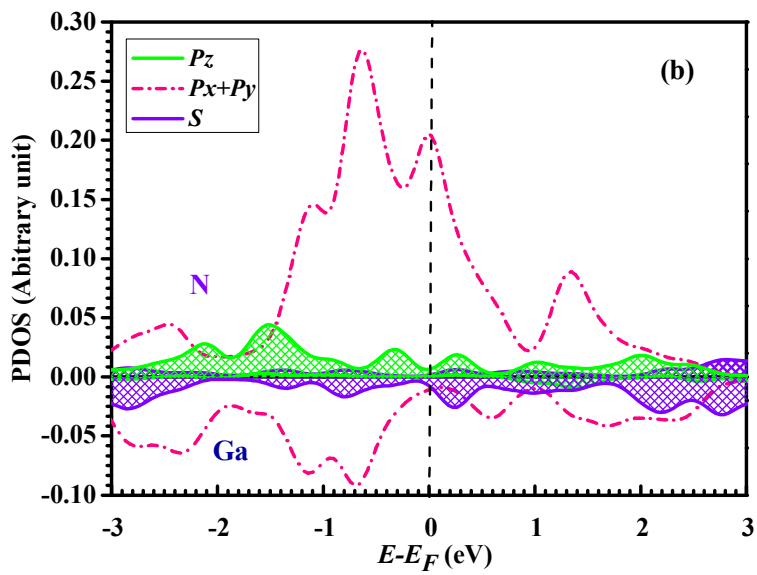
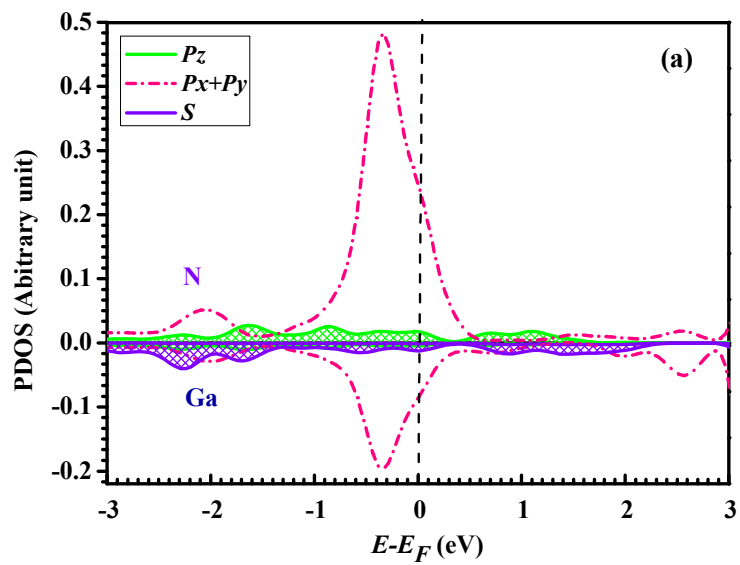


Fig. 5. Transmission coefficient as a function of energy for GaN molecule at optimal position under different external bias: (a) top-top configuration, (b) hollow-top configuration, (c) top-hollow configuration, and (d) hollow-hollow configuration.



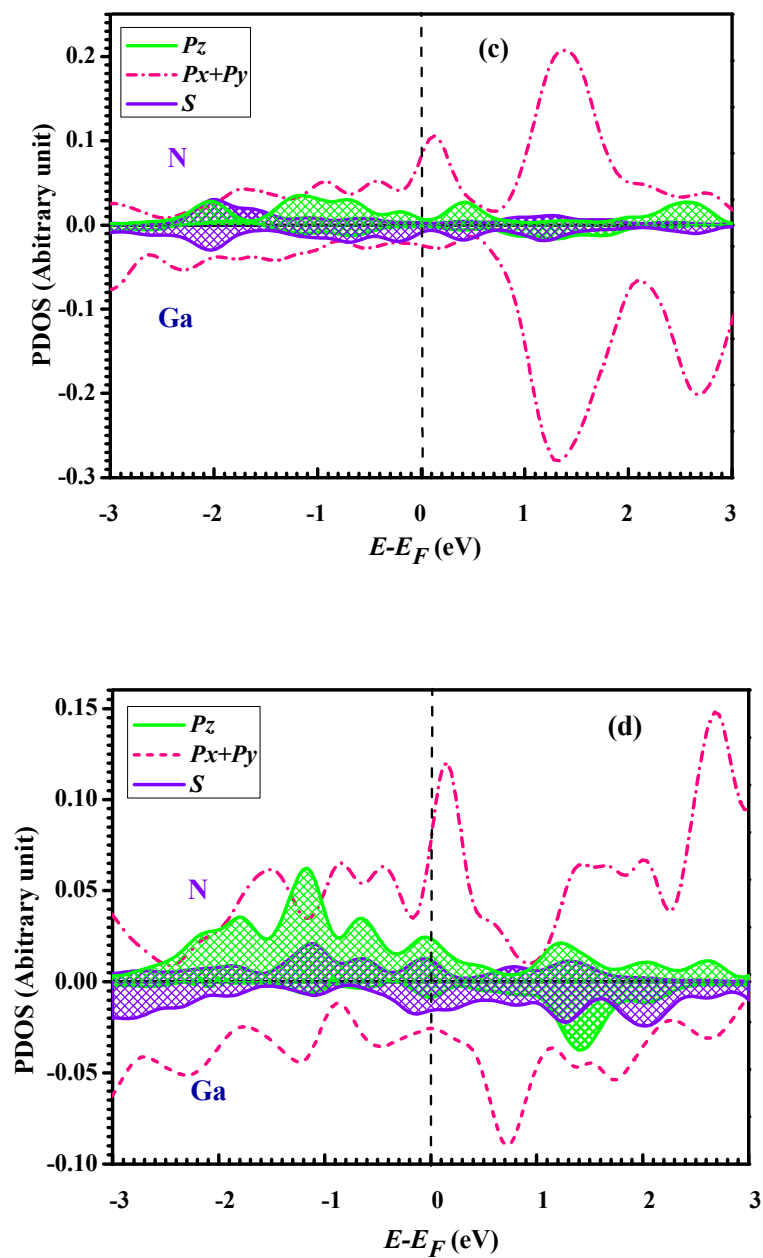


Fig. 6. The projected density of state (PDOS) for GaN molecule at optimal position: (a) top-top configuration, (b) hollow-top configuration, (c) top-hollow configuration, and (d) hollow-hollow configuration.

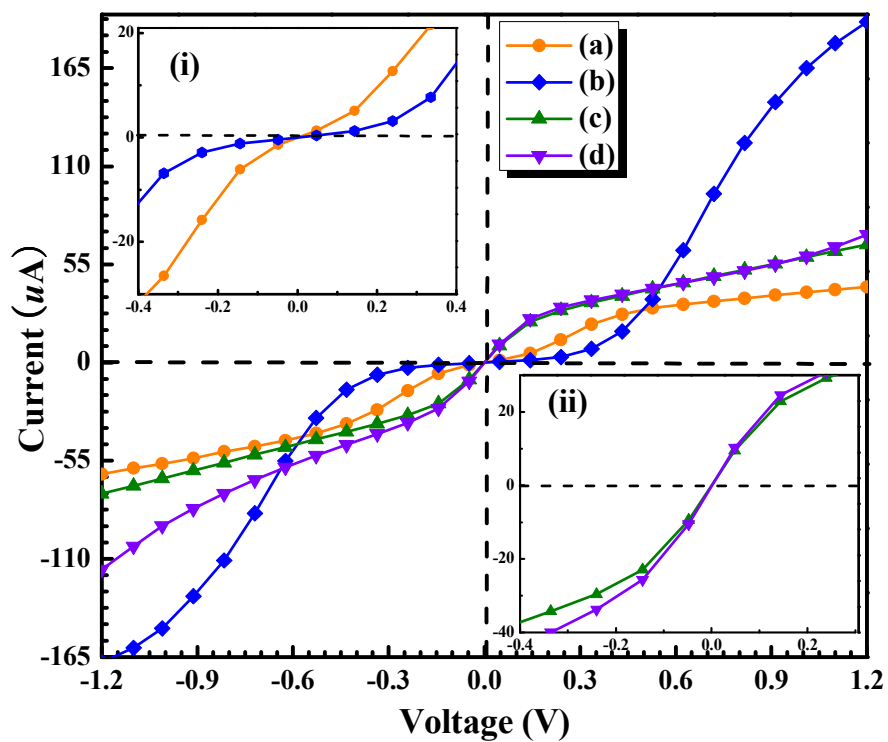


Fig. 7. I - V curves calculated for four configurations between the GaN molecule and the electrodes at the equilibrium positions: (a) top-top configuration, (b) hollow-top configuration, (c) top-hollow configuration, and (d) hollow-hollow configuration.